Sensors and Materials, Vol. 34, No. 12 (2022) 4451–4462
MYU Tokyo

S & M 3121

Extraction of Earthquake Damage Information and Mapping of Buildings from Single Post-earthquake Polarimetric Synthetic Aperture Radar Image Based on Polarimetric Decomposition and Texture Features

Wei Zhai,[1,2,3,4] Xiaoqing Wang,[1*] Yaxin Bi,[2**]
Jun Liu,[5] Guiyu Zhu,[3,4] and Jianqing Du[3,4]

[1]Institute of Earthquake Forecasting, China Earthquake Administration, Beijing, China
[2]Faculty of Computing, Engineering and the Built Environment, Ulster University, Belfast, United Kingdom
[3]Lanzhou Institute of Seismology, China Earthquake Administration, Lanzhou, China
[4]Lanzhou Institute of Geotechnique and Earthquake, China Earthquake Administration, Lanzhou, China
[5]National Earthquake Response Support Service, Beijing, China

(Received October 24, 2022; accepted November 21, 2022)

Keywords: buildings, earthquake damage assessment, polarimetric decomposition, PolSAR, texture features

The collapse of buildings caused by destructive earthquakes often leads to severe casualties and economic losses. After an earthquake, an accurate assessment of building damage will be essential in making plans of emergency responses. Four-polarimetric synthetic aperture radar (PolSAR) data have advantages over synthetic aperture radar (SAR) imaging data, because they are not occluded by sunlight or clouds. They also contain the most abundant information of four polarimetric channels. Therefore, a single PolSAR image can be used to identify post-earthquake building damage. It is easy to overestimate the number of collapsed buildings and the degree of damage by earthquakes when using only a traditional polarimetric decomposition method for PolSAR data. In urban areas, buildings can stand in parallel in typical SAR imaging with strong scattering features, and there are also some oriented standing buildings with lower scattering intensity or similar scattering characteristics to collapsed buildings; thus, these oriented standing buildings are often misconstrued as collapsed buildings. In this study, we propose a new texture feature, namely, the mean standard deviation (MSD) index based on the gray-level co-occurrence matrix (GLCM), to solve the overestimation of building damage caused by earthquakes. Moreover, on the basis of the improved Yamaguchi four-component decomposition method and the MSD index, we develop a method of identifying the damage of buildings using only a single post-earthquake PolSAR image. In our study case, 75000 undamaged and damaged building samples are used in the experiment. The proposed method has greatly improved the accuracy and reliability of extracted building damage information. The experimental results show identification accuracies of 82.43 and 80.30% for damaged and undamaged buildings, respectively. Compared with the traditional polarimetric decomposition method, 66.89% standing buildings are successfully isolated from the mixture of collapsed buildings using our method.

*Corresponding author: e-mail: wangxiaoq517@163.com
**Corresponding author: e-mail: y.bi@ulster.ac.uk
https://doi.org/10.18494/SAM4188

1. Introduction

Over the past decade, earthquakes have occurred frequently throughout the world, and devastating earthquakes have caused huge losses of human life and property.[1] In urban areas, post-earthquake casualties are mainly caused by the collapse of buildings.[2] In the search and rescue of people buried in rubble, the sooner the information about the collapse of buildings is obtained, the more likely it is that people will survive.[3] Therefore, after an earthquake, one of the high-priority tasks will be calculating the distribution of collapsed buildings in the earthquake region quickly and accurately. This information will provide a guideline for making emergency plans for response to an earthquake.[4] Traditionally, the main method of obtaining post-earthquake damage information has been through field survey. Although information obtained by this method is highly credible, this method often has a heavy workload and low efficiency over a large area.[5] Remote sensing technology enables the swift monitoring of the disaster situation over a large range; thus, it has become an important means of earthquake emergency response and post-earthquake disaster assessment.[6] Because earthquakes tend to occur at night or are often accompanied by clouds, rain, snow, and other severe weather conditions, optical remote sensing is not always effective.[7] In contrast, as radar waves are highly penetrable and unaffected by sunlight, they can easily pass through thick clouds to obtain information from disaster areas.[8] Synthetic aperture radar (SAR) remote sensing can effectively obtain ground images under various weather conditions.[9] After an earthquake, radar remote sensing is reliable for monitoring disasters. In the past, multitemporal pre-earthquake and post-earthquake SAR data were often collected after an earthquake for use in estimating the difference between post-earthquake and pre-earthquake situations and in determining the affected location. However, because it is labor-intensive to collect pre-earthquake SAR data, there is almost no pre-earthquake data archived in most remote areas. In this study, we only use the single-temporal post-earthquake SAR data to identify the degree of damage of buildings in disaster areas, whereby we can avoid the multitemporal data registration operation.[10] Four-polarimetric SAR (PolSAR) data contain more information than remote sensing data of a single-polarimetric or dual-polarimetric radar, because PolSAR data comprise four polarimetric channels: HH, HV, VH, and VV, where H represents horizontal polarization and V represents vertical polarization. In cases where only the single post-earthquake SAR data can be used for assessing post-earthquake building damage, we select to use PolSAR data to achieve a higher accuracy of damage identification and a more reliable post-earthquake damage assessment.[11]

With the increasing abundance of PolSAR data sources, many scholars have applied PolSAR to post-earthquake disaster identification because of its effectiveness in identifying ground objects.[12–14] In remote areas, it is difficult to obtain PolSAR data sources in pre-earthquake images, but the information contained in PolSAR data is sufficient for the task of damage identification of earthquakes based on single-temporal data; hence, recently, a continuously increasing number of scholars are beginning to use only the single-temporal post-earthquake data to identify the damage of buildings. Moreover, many experiments show that the identification results of this method can meet the accuracy and speed requirements of earthquake damage identification, and the identification accuracy is comparable to that of multitemporal

SAR data.[15,16] Since polarimetric features are the main information source of PolSAR data, the extraction of information of damaged buildings from single-temporal post-earthquake PolSAR data is mainly based on the polarimetric target decomposition model and polarimetric features parameters.[17–19] However, because texture features of PolSAR images are as important as polarimetric features in PolSAR data, they have an even higher identification efficiency than polarimetric features in many cases. Therefore, many scholars identify the damage of buildings from the texture features when using the polarization information in PolSAR data; this can yield better identification results of building damage caused by earthquakes.[20,21] More recently, with the rapid advancement of deep learning technologies, many scholars have used convolutional neural network (CNN) algorithms to integrate various polarimetric and texture features of PolSAR data to identify building damage caused by earthquakes.[22]

After a destructive earthquake, the collapse of building walls results in the damage of dihedral structures formed between the walls and the ground, so that double-bounce scattering characteristics of SAR images with higher scattering intensity cannot be formed; then, the scattering mechanism is no longer dominated by double-bounce scattering, but rather by volume scattering. Because of this characteristic, collapsed buildings would have a lower scattering intensity than standing buildings. However, there is also a unique phenomenon in SAR images: the orientation of some standing buildings is not parallel to the SAR flight path. Such buildings are called oriented buildings. Since the polarization basis of oriented buildings is rotated, such buildings have a strong depolarization effect, and their predominant scattering mechanism is volume scattering, making their scattering intensity low. Therefore, oriented and collapsed buildings have similar scattering mechanisms and scattering intensities and are easily confused in SAR images, which often results in the excessive assessment of damaged buildings. To solve this problem, we propose a novel texture feature parameter based on the statistical texture features of PolSAR data, namely, the mean standard deviation (MSD) index of texture features, in this paper. The MSD index is used to design an identification scheme for assessing the degree of building damage caused by earthquakes. Our experimental results show that the use of the proposed MSD index can significantly improve the accuracy of identifying post-earthquake building damage. The research design and experiment will be detailed in the following sections.

2. Materials and Methods

2.1 Study earthquake and data

In this study, the Ms7.1 Yushu earthquake, which occurred in Yushu County, Qinghai Province, China on April 14, 2010, is used as the case study. The epicenter of the earthquake was at 33.1°N, 96.6°E. Yushu County is at a high altitude and has a dry and cold climate. The urban area has a small amount of sparsely distributed vegetation, which has little influence on building identification in the earthquake region. Therefore, the vegetation type was not considered in this experiment. The boundary .shp data of Yushu County was used to mask the mountains around the urban area, and the experiment of extracting information of building damage caused by the earthquake was carried out only for the urban area.

The experimental data are obtained from P-band airborne high-resolution PolSAR images acquired using the Chinese airborne SAR mapping system SARMapper on 15 April 2010, one day after the earthquake. The range and azimuth spatial resolutions of the experimental data are both about 1 m. The illumination direction is upward from the bottom, and the SAR flight path is level flight from east to west. Figure 1 shows the Pauli RGB image of the PolSAR data used for the experiment. The Pauli RGB image is a color composite image with (|HH-VV|) as the red band, (|HV|) as the green band, and (|HH+VV|) as the blue band, and the image is composed of 8192 × 4384 pixels. To verify the accuracy of the proposed method, 25000 samples are selected from Google Earth for collapsed, oriented, and parallel buildings respectively marked in red, blue, and green in Fig. 1.

2.2 Polarimetric decomposition method

The polarimetric decomposition method can decompose different scattering components. In a post-earthquake PolSAR image, different scattering components correspond to buildings in different states. For example, for a standing building that is parallel to the SAR flight path, the dominant scattering components are double-bounce scattering components; thus, the resulting identification of the building in the earthquake region can be directly accomplished by the polarimetric decomposition method. On the other hand, both the collapsed buildings in the earthquake region and the standing buildings, as oriented buildings, have predominantly volume scattering components. In our research design, to identify standing buildings (including parallel and oriented buildings) more completely, the improved Yamaguchi four-component decomposition (IYFD) method[23] was adopted for the polarimetric decomposition of PolSAR data. The IYFD method was developed by Yamaguchi *et al.*[23] by improving the Yamaguchi

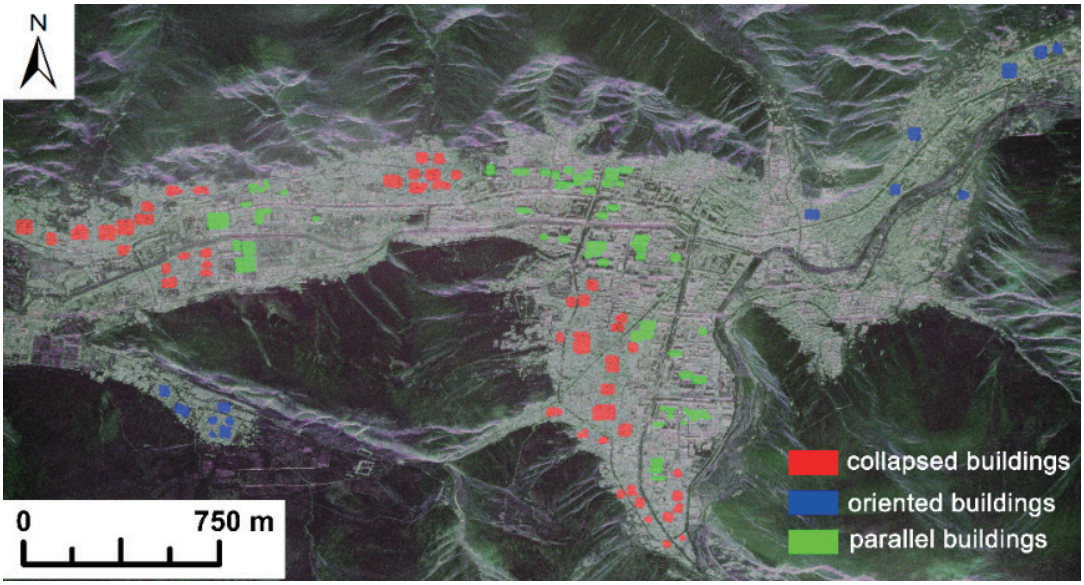

Fig. 1. (Color online) Pauli RGB color composite image of the urban area in Yushu County with marked verification samples of three types of buildings in earthquake region.

four-component decomposition model to enhance the identification accuracy of oriented buildings with the aim of identifying oriented buildings completely and accurately.(23)

2.3 MSD index of texture feature

The volume scattering components produced by the polarimetric decomposition method can be used to render oriented and collapsed buildings. It can be seen from Fig. 2 that histogram curves of the total intensity of PolSAR data for the oriented and collapsed buildings highly overlap. This indicates that the scattering intensities of the two types of buildings are significantly similar. Although they have similar scattering mechanisms and scattering intensities, they still have different texture features in PolSAR images. The oriented buildings have a regular and finer texture, while the collapsed buildings have a more messy and coarse texture. The texture feature index can better reflect the difference in scattering characteristic between the two types of damaged buildings, thereby distinguishing them. We have designed a feature parameter, the MSD index, that can be applied to classify and identify the two types of buildings in earthquake zones, improve the overclassification phenomenon of collapsed buildings, and restrain the overcorrection of oriented buildings. The MSD index can reveal the texture differences between the oriented and collapsed buildings to identify these buildings accurately. It can be seen from Fig. 2 that the MSD indices of the oriented buildings are generally smaller than those of the collapsed buildings. Compared with the total intensity of PolSAR data without extracting texture features, the use of the MSD index enables a better identification of the two types of buildings.

The total power of a PolSAR image (termed SPAN image) comprises the intensity information of all polarimetric channels. The SPAN image contains the most intensity information. Therefore, we use the SPAN image to calculate the MSD index of PolSAR data. The calculation method of SPAN is as follows:

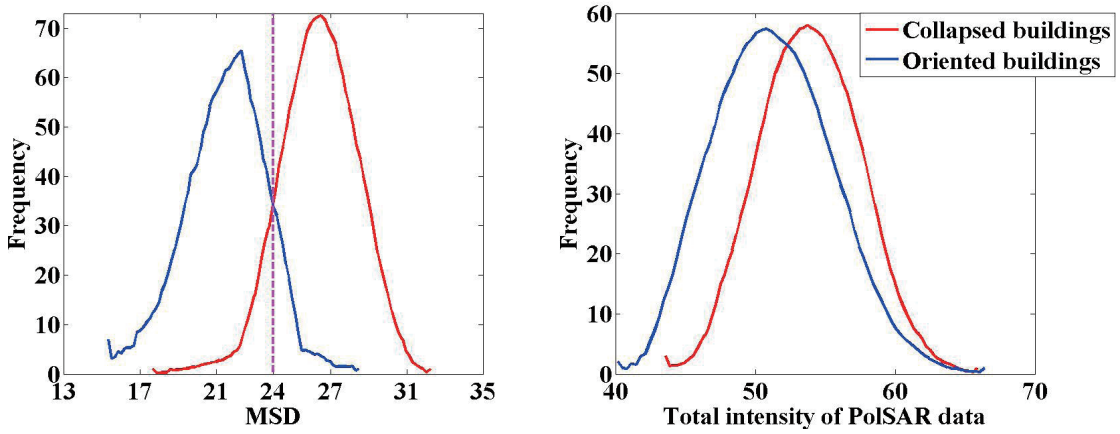

(a) (b)

Fig. 2. (Color online) Histograms of (a) MSD index and (b) total intensity of PolSAR data for oriented and collapsed buildings.

$$SPAN = \mathrm{HH}^2 + \mathrm{HV}^2 + \mathrm{VH}^2 + \mathrm{VV}^2, \tag{1}$$

where HH represents the horizontal-to-horizontal (H-H) polarization combinations for transmitting and receiving H signals, HV denotes the cross-polarized combinations (H-V) with transmitting H and receiving V signals, VH denotes the cross-polarized combinations (V-H) with transmitting H and receiving V signals, and VV represents vertical-to-vertical (V-V) polarization combinations for transmitting V and receiving V pulses. The gray-level co-occurrence matrix (GLCM)[24] is a very popular and widely used texture feature extraction method based on statistical methods. In general, the eight commonly used second-order statistical texture parameters of GLCM-based texture features are *mean*, *variance*, *contrast*, *homogeneity*, *entropy*, *dissimilarity*, *correlation*, and *second moment*. We propose to define the MSD index of the texture feature using the features of mean and variance as follows:

$$MSD = mean\left(SPAN\right) - \sqrt{variance\left(SPAN\right)}, \tag{2}$$

where *mean*(•) and *variance*(•) represent the mean and variance values calculated on the basis of GLCM for (•), respectively. The specific calculations of mean and variance are detailed in Ref. 24.

2.4 Identification of building damage due to earthquake

As shown in Fig. 3, the process of extracting the information of damaged buildings mainly includes four steps. Firstly, the improved Yamaguchi four-component decomposition method is used for the polarimetric decomposition of PolSAR data to extract the double-bounce and volume scattering components. Secondly, the ground objects to be identified in the PolSAR image corresponding to the double-bounce components are classified as parallel buildings. Thirdly, the SPAN image of the PolSAR data is calculated and extracted using Eq. (1), and the MSD values of the PolSAR data are calculated using Eq. (2). Fourthly, an appropriate threshold value is selected for the MSD index. According to the classification rules shown in Eq. (3), the collapsed and oriented buildings are classified on the basis of the volume scattering components obtained by polarimetric decomposition. It can be seen from Fig. 2 that the overall MSD values of the collapsed buildings are greater than those of the oriented buildings. Therefore, the classification rules of the MSD index can be expressed as

$$\begin{aligned} &x \in \text{volume\_dominated buildings} \\ &\quad \text{if } MSD \geq \varepsilon \\ &\quad\quad x \in \text{collapsed buildings}, \\ &\quad \text{if } MSD < \varepsilon \\ &\quad\quad x \in \text{oriented buildings}, \end{aligned} \tag{3}$$

where ε represents a threshold value for classifying collapsed and oriented buildings using the MSD index. ε is calculated as

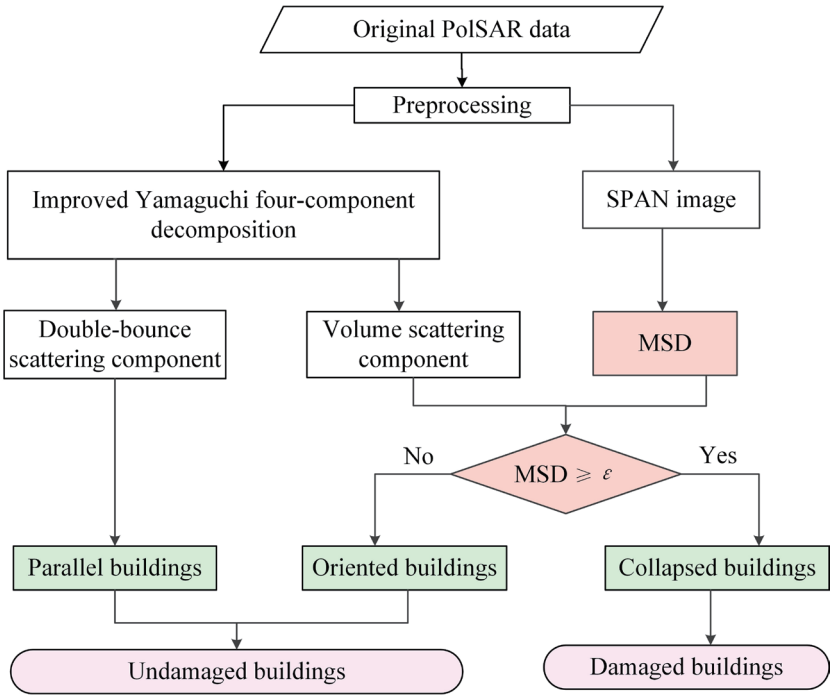

Fig. 3. (Color online) Flowchart for extracting information of building damage caused by earthquakes.

$$\varepsilon = \frac{mean(CB) + mean(OB)}{2}, \tag{4}$$

where *mean*(•) represents the calculated average value of (•), and CB and OB represent the collapsed and oriented building sample sets, respectively. Finally, the oriented and parallel buildings are combined into undamaged buildings, and the collapsed buildings are defined as a category of damaged buildings.

3. Results

By the identification process of post-earthquake building damage shown in Fig. 3, the damaged and undamaged buildings in the PolSAR data were extracted in this experiment. The classification parameters, i.e., the MSD indices, of collapsed and oriented buildings in the PolSAR data were calculated using Eq. (2), and the two types of buildings were classified in accordance with Eq. (3). Using Eq. (4), the classification threshold ε of the two types of buildings was calculated with the collapsed and oriented building sample sets marked in Fig. 1. The calculated ε is 23.90, which is basically consistent with the value of 24 at the boundary of MSD histogram curves of the collapsed and oriented buildings shown in Fig. 2. Therefore, in this experiment, when the MSD index was used to classify the collapsed and oriented buildings on the basis of Eq. (3), the classification threshold ε was set as 23.90.

The result of extracting damage information for buildings is shown in Fig. 4. The experimental result only presents the building damage in the urban area after the mountains around the urban area were masked by the urban boundary data of Yushu County. Using the verification samples of collapsed, oriented, and parallel buildings marked in Fig. 1, we evaluated the accuracies of the proposed method for identifying post-earthquake building damage. The experimental results are shown in Fig. 4 and the confusion matrix of classification accuracy is presented in Table 1. It can be seen from Table 1 that the total number of diagonal samples in which the experimental results are consistent with the reference samples accounts for 80.65% of the total samples. Therefore, the overall accuracy of the identification of the three types of buildings in the study area by the proposed method is 80.65%.

4. Discussion

From Table 1, we can see that the accuracy of identifying damaged buildings, i.e., the correct identification rate of collapsed buildings, by extracting the damage information of the buildings by the proposed method is 82.43%, and the accuracy of identifying undamaged buildings, i.e.,

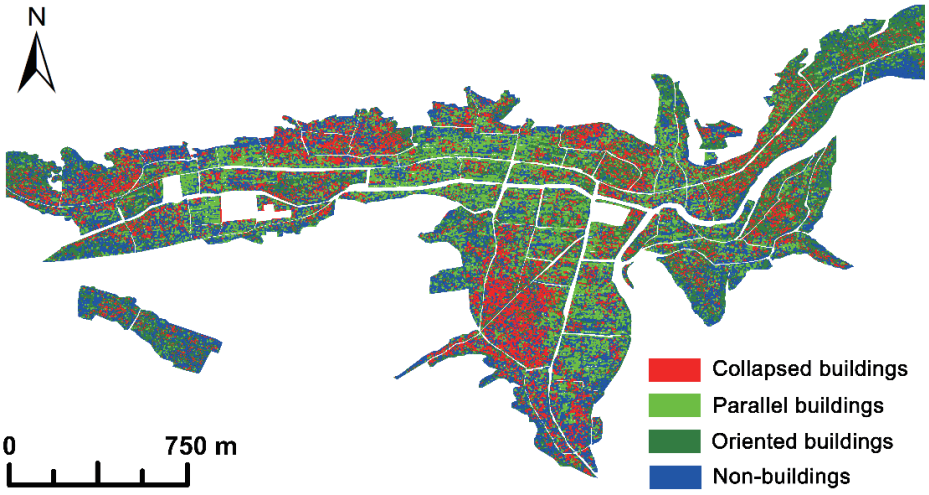

Fig. 4. (Color online) Extraction results of three types of buildings after earthquake in Yushu County.

Table 1
Confusion matrix for evaluating accuracy of identification of three types of buildings.

	Experiment		
	CB	OB	PB
	(No. of samples)		
Reference			
CB	20608	4392	0
OB	8293	16717	0
PB	1566	268	23166
	OA: 80.65%		

OA, CB, OB, and PB represent overall accuracy, collapsed buildings, oriented buildings, and parallel buildings, respectively.

the comprehensive correct identification rate for oriented and parallel buildings, is 80.30%. That is, the identification accuracies for damaged and undamaged buildings are both above 80%. The identification results are fairly balanced for damaged and undamaged buildings. The experimental results show neither the underestimation of undamaged buildings due to the overestimation of damaged buildings nor the overestimation of the number of undamaged buildings due to the underestimation of the number of damaged buildings. Therefore, the identification results obtained by the method proposed herein are effective for assessing building damage after earthquakes, because an excessive identification of damaged buildings will lead to a waste of rescue resources, while an inadequate identification of damaged buildings will delay the timely rescue of buried persons, which may be very tragic.

Among the oriented building samples, 66.89% were successfully identified from the volume scattering components, which is the ratio of oriented buildings correctly classified into the set of oriented building samples. If these oriented buildings were misclassified as collapsed buildings, great amounts of rescue manpower and materials would be incorrectly allocated. All the corresponding ground objects of the volume scattering components are classified as collapsed buildings when using the traditional IYFD method. Although this method can achieve a 99.92% identification rate of collapsed buildings, the rate of correctly identifying undamaged buildings is only 46.33%. Therefore, when the traditional IYFD method is used to identify the damage of buildings, an inaccurate classification of the volume scattering components will sharply reduce the correct identification rate of undamaged buildings in order to improve the correct identification rate of collapsed buildings.

Most collapsed and oriented buildings are misclassified at the boundary of the two different types of ground objects or at the edges of a certain type of ground object; the interfaces of different ground objects are often only 1–2 pixels wide. When the MSD index is applied, it is easy to jointly calculate the statistical features of the two types of ground objects at their boundaries because of the domain effect. Thus, the MSD values of the two types of ground objects are usually similar or the same, such that one type of ground object might easily be classified into the other type of ground object. Parallel buildings are misclassified as collapsed and oriented buildings because the scattering intensities of the transition areas of some roof areas and some layover and shadows are weak. The areas of parallel buildings with low scattering intensity are easily misclassified as collapsed and oriented buildings that are dominated by the volume scattering mechanism. It can be seen from Table 1 that the number of parallel buildings misclassified as collapsed buildings is much larger than that of parallel buildings misclassified as oriented buildings because there are many residual walls that can form dihedral structures with the ground in the case of collapsed buildings. The scattering intensity of such collapsed residual walls is higher than that of oriented buildings. Therefore, it is easier to misclassify parallel buildings with high scattering intensity as collapsed residual walls with high scattering intensity. In addition, the causes of the misclassification of the three types of buildings also include the errors produced by the manual selection of the verification samples. For example, in a complete verification sample block, there may be other scattered ground object samples not belonging to the verification sample category. In other cases, it is easy for other ground objects to appear at the edges of the selected building samples.

Because the MSD values of oriented buildings are generally less than those of collapsed buildings, if the segmentation threshold value of the MSD index is set to be smaller, the identification accuracy of collapsed buildings will be higher, and more collapsed buildings will be misclassified as oriented buildings. As a result, the number of collapsed buildings will be overestimated and that of standing buildings will be underestimated. To the contrary, if the segmentation threshold value of the MSD index is set to be larger, fewer collapsed buildings will be identified and the identification of the damaged areas of the buildings will more easily fail, which may delay rescue and incur great risks to the emergency rescue plan. Therefore, the segmentation threshold value of the MSD index between the oriented and collapsed buildings should not be set too small merely to obtain a high identification accuracy for oriented buildings. The segmentation threshold value of the MSD index should be set appropriately on the premise of ensuring that the correct identification rate of collapsed buildings is not less than 80%, thereby ensuring that the correct identification rate of oriented buildings is also above 80%.

5. Conclusions

To avoid the overclassification of collapsed buildings caused by the traditional IYFD method, the MSD index, which can describe the difference in texture feature between the collapsed and oriented buildings, was proposed in this study. The proposed MSD index can better distinguish the two types of buildings with the same dominant scattering mechanism, namely, volume scattering. The MSD index can well identify the difference in spatial distribution texture between the collapsed and oriented buildings. Therefore, in this work, the MSD index was used to distinguish a large number of oriented buildings incorrectly classified as collapsed buildings by the traditional IYFD method, thus improving the identification accuracy in the assessment of building damage caused by earthquakes. The MSD index of the SPAN image was calculated and used to further separate the volume scattering components produced by the improved Yamaguchi four-component decomposition of the PolSAR data into the collapsed and oriented buildings on the basis of the MSD threshold value. In this work, the MSD classification threshold value was automatically calculated referrring to the statistical characteristic of the sample space without any manual intervention. This method improves the degree of automation of the algorithm and simplifies the selection process of the threshold value. It also reduces the errors accompanying the manual selection of the threshold value and improves the performance of the algorithm. This method overcomes the issue of damage overidentification wherein all the volume scattering components generated from the improved Yamaguchi four-component decomposition are directly classified as collapsed buildings. The experimental results showed that the proposed extraction method of building damage can well identify the damaged and undamaged buildings in an earthquake-stricken region with a high identification accuracy of 80.65% for damaged buildings. 66.89% of the oriented buildings were successfully separated from the collapsed buildings identified by the traditional IYFD method, obviously improving the extraction accuracy of building damage information. Because of the limited amount of data available, there are no more experimental data available for use in this experiment at present. When more data become available in the future, we will further verify the robustness of the proposed method. In

further improvement work, we will try to classify some uncertain areas of the collapsed and oriented buildings using different damage levels: most likely to be a collapsed building area, highly likely to be a collapsed building area, less likely to be a collapsed building area, and probably not a collapsed building area. In this way, the risk of some collapsed buildings being misidentified as undamaged buildings can be reduced.

Acknowledgments

This work was supported by the National key R&D program of China (No. 2017YFB0504104); the Gansu Province Science and Technology Program (22JR5RA822); the National Natural Science Foundation of China (41601479; 42061073); the Key Talent Project of Gansu Province (11276679015); the Dragon 5 programme (ID: 59308), a collaboration between the European Space Agency and the Ministry of Science and Technology of China; the High Score Project of State Administration of Science, Technology and Industry for National Defense (Phase II): Application of remote sensing based seismic intensity and loss assessment (31-Y30F09-9001-20/22-12); the Science for Earthquake Resilience of China Earthquake Administration (XH18049); the Basic Research Project of Institute of Earthquake Science, China Earthquake Administration (2021IESLZ4); the Gansu Earthquake Administration innovation team special fund (2019TD-01-02); the State Scholarship Fund of China Scholarship Council (CSC); and the Earthquake Science and Technology Development Fund Program of Lan-zhou Earthquake Research Institute, China Earthquake Administration (2015M02).

References

1 S. Karimzadeh and M. Matsuoka: Remote Sens. **13** (2021) 12. https://doi.org/10.3390/rs13122267
2 M. Matsuoka and F. Yamazaki: Remote Sens. **4** (2010) 1. https://doi.org/10.1117/1.3525581
3 R. Gonzalez-Drigo, E. Cabrera, G. Luzi, L. G. Pujades, Y. F. Vargas-Alzate, and J. Avila-Haro: Remote Sens. **11** (2019) 23. https://doi.org/10.3390/rs11232830
4 Z. Stojadinovic, M. Kovacevic, D. Marinkovic, and B. Stojadinovic: Earthq. Spectra **38** (2022) 1. https://doi.org/10.1177/87552930211042393
5 M. Hasanlou, R. Shah-Hosseini, S. T. Seydi, S. Karimzadeh, and M. Matsuoka: Remote Sens. **13** (2021) 6. https://doi.org/10.3390/rs13061195
6 V. Oludare, L. Kezebou, O. Jinadu, K. Panetta, and S. Agaian: Proc. SPIE 12100 Conf. (2022) 121000L-1. https://doi.org/10.1117/12.2618901
7 P. L. Ge, H. Gokonb, and K. Meguro: Remote Sens. Environ. **240** (2020) 111693. https://doi.org/10.1016/j.rse.2020.111693
8 R. Cossu, F. Dell'Acqua, D. A. Polli, and G. Rogolino: IEEE J-stars **5** (2012) 4. https://doi.org/10.1109/JSTARS.2012.2185926
9 A. F. S. Putri, W. Widyatmanti, and D. A. Umarhadi: Remote Sens. Appl. **26** (2022) 100724. https://doi.org/10.1016/j.rsase.2022.100724
10 C. Wang, Y. Zhang, T. Xie, L. Guo, S. S. Chen, J. Y. Li, and F. Shi: Remote Sens. **14** (2022) 5. https://doi.org/10.3390/rs14051100
11 X. L. Sun, X. Chen, L. Yang, W. S. Wang, X. X. Zhou, L.L. Wang, and Y. Yao: Remote Sens. **14** (2022) 13. https://doi.org/10.3390/rs14133009
12 M. Jung, M. Chung, and Y. Kim: Int. Arch. Photogramm. Remote Sens. Spatial Inf. Sci. (Gi4DM 2019) 181–185. https://doi.org/10.5194/ISPRS-ARCHIVES-XLII-3-W8-181-2019
13 S. E. Park and Y. T. Jung: Remote Sens. **12** (2020) 1. https://doi.org/10.3390/rs12010137
14 E. Ferrentino, F. Nunziata, C. Bignami, L. Graziani, A. Maramai, and M. Migliaccio: Int. J. Remote Sens. **42** (2021) 15. https://doi.org/10.1080/01431161.2021.1933247

15 P. Mazzanti, S. Scancella, M. Virelli, S. Frittelli, V. Nocente, and F. Lombardo: Remote Sens. **14** (2022) 9. https://doi.org/10.3390/rs14092210
16 W. Zhai, H. F. Shen, C. L. Huang, and W. S. Pei: Remote Sens. **8** (2016) 3. https://doi.org/10.3390/rs8030171
17 H. Miao, X. Q. Wang, L. Ding, and X. Ding: Proc. 2021 IEEE Int. Geoscience and Remote Sensing Symp. Conf. (IGARSS 2021) 8566–8569. https://doi.org/10.1109/IGARSS47720.2021.9555084
18 W. Zhai, C. L. Huang, and W. S. Pei: Remote Sens. **10** (2018) 10. https://doi.org/10.3390/rs10101613
19 W. Zhai, J. F. Zhang, X. L. Xiao, J. H. Wang, H. R. Zhang, X. X. Yin, and Z. Wu: Remote Sens. Lett. **12** (2021) 6. https://doi.org/10.1080/2150704X.2021.1906975
20 W. Zhai, C. L. Huang, and W. S. Pei: Remote Sens. **11** (2019) 8. https://doi.org/10.3390/rs11080897
21 Q. H. Chen, H. Yang, L. L. Li, and X. G. Liu: IEEE J-stars **13** (2020) 154. https://doi.org/10.1109/JSTARS.2019.2954292
22 Y. B. Bai, C. Gao, S. Singh, M. Koch, B. Adriano, E. Mas, and S. Koshimura: IEEE Geosci. Remote Sens. Lett. **15** (2017) 1. https://doi.org/10.1109/LGRS.2017.2772349
23 Y. Yamaguchi, A. Sato, W. M. Boerner, R. Sato, and H. Yamada: IEEE Trans. Geosci. Remote Sens. **49** (2011) 6. https://doi.org/10.1109/TGRS.2010.2099124
24 R. M. Haralick, K. Shanmugam, and I. H. Dinstein: IEEE Trans. Syst., Man Cybern. SMC-3 (1973) 610. https://doi.org/10.1109/TSMC.1973.4309314